Transplant Immunology 53 (2019) 61–71

Contents lists available at ScienceDirect

Transplant Immunology

journal homepage: www.elsevier.com/locate/trim

Evaluation of the host immune response and functional recovery in peripheral nerve autografts and allografts

Kelly Cristine Santos Roballo, Jared Bushman*

University of Wyoming, School of Pharmacy, Laramie, WY 82072, USA

ARTICLE INFO

Keywords:
Local immune system
Transplant
Peripheral nerve

ABSTRACT

Allogeneic peripheral nerve (PN) transplants are an effective bridge for stimulating regeneration of segmental PN defects, but there are currently no detailed studies about the timeline and scope of the immunological response for PN allografting. In this study, the cellular immune response in PN allografts and autograft was studied during the acute and chronic phases of a 1.0 cm critical size defect in the rat sciatic nerve at 3, 7, 14, 28 and 98 days after grafting autologous or allogeneic nerves without any immunosuppressive treatment. The assessment was based on functional, histomorphometrical and immunohistochemical criteria. Results showed modestly better functional outcomes for autografts with coordinate and adaptive immune response represented by the presence of CD11c, CD3, CD4, NKp46 and CD8 cells at 3 days, CD45R positive cells and CD25 positive cells at seven and CD45R positive cells at 14 days which seems an adaptive immune response. In contrast, allograft in the early time points showed innate immune response instead of adaptive immune response until day 14, when there was some increase in cell-mediated immunity. In conclusion, in PN autografts the immune system is synchronic initiating with a more robust early innate response that more rapidly transitions to adaptive while for PN allografts the infiltration of immune cells is slower and more gradually progresses to a moderate adaptive response.

1. Introduction

PNs are primarily composed of axons, Schwann cells (SCs), resident immune cells and connective tissue [1]. When PNs are injured, the principal outcomes are loss and aberration of function, which can be permanent and lead to lifelong disability [2]. In severe cases, termed neurotmesis by the Seddon and Sunderland classification, a nerve is completely bisected and functionality is immediately lost distal to the injury [3,4]. Wallerian degeneration occurs distal to the injury as SCs dissociate from axons and the axons break down and are degraded [5,6]. The result of Wallerian degeneration leaves the distal segment devoid of functional axons but primed for axons to reenter and for regeneration to occur [5,6]. Functional regeneration requires that surviving proximal axons extend into the distal PN segment and regenerate to their target motor and sensory tissues [5,6].

For segmental defects greater than ~0.5 cm, a bridging device must be placed between the stumps in order for proximal axons to effectively regenerate into the distal segment. Autografted PNs, typically sensory segments of the sural or forelimb cutaneous nerves, are the gold standard for the bridging device. Biodegradable conduits and wraps are also clinically used but are fractionally effective compared to autografts, especially for larger defects [7]. Allogeneic PN grafts are as or more effective than autografts owing to that they can be mixed (motor and sensory axons) and more exactly matched for size and complex nerve structures [8]. PN allografts, however, are rarely used clinically due to the risks associated with immunosuppressive therapy used with allogeneic tissue grafts [9]. Improvements in immunosuppressive therapy that reduce or remove risks may enable more the widespread use of this very effective PN regeneration strategy.

While many reports show endpoint histology after PN allografts as compared to autografts, there are currently no detailed studies on the immunological response to PN allografts in the acute and chronic phases. In an effort to characterize the cellular processes occurring during the acute and chronic phases, we compared 1.0 cm critical size defects grafted with autologous or allogeneic PNs without immunosuppressive therapy in a rat sciatic nerve model. Tissue was collected 3, 7, 14, 28 and 98 days (fourteen weeks) after grafting for histology and stained for markers of macrophages, dendritic, T cells, B cells, Natural Killers, Schwann cells and axons. Functional outcomes of compound muscle action potentials (CMAPS) and muscle mass were also collected. The results indicate a substantial degree of regeneration with allografts in the absence of immunosuppression, but shows

* Corresponding author.
E-mail address: jbushman@uwyo.edu (J. Bushman).

https://doi.org/10.1016/j.trim.2019.01.003
Received 27 August 2018; Received in revised form 24 January 2019; Accepted 25 January 2019
Available online 05 February 2019

distinctions in the types, quantities and timing of immune cell infiltration between autograft and allograft. It is anticipated that these studies may be used as a basis of comparison for future studies assessing the efficacy of PN allografting.

2. Objective

The objective of these studies was to more fully characterize the immunological response to allogeneic PN grafts in vivo. To do this, the cellular immune response to PN damage was studied during acute and chronic phases following the insertion of a 1.0 cm PN autograft or allograft in the rat sciatic nerve. Assessment of immune cell response and nerve regeneration was based on functional, histomorphometrical and immunohistochemical criteria from tissue harvested on days 3, 7, 14, 28 and 98 after surgery.

3. Material and methods

3.1. Study design

All experiments were conducted in accordance with the University of Wyoming Institutional Animal Care and Use Committee under approved and current protocols. Female Lewis (LEW- $RT1^l$) rats (Charles River Laboratories, Massachusetts, USA), 200–230 g, were submitted to sciatic nerve transection surgery and were recipients of autograft (Auto) or allograft (Allo) transplantation. Donor PN tissue for allografts was harvested from deceased female Sprague–Dawley (SD—$RT1^b$) rats (Charles River Laboratories, Massachusetts, USA), 200–230 g (Table 1). For bulk cell infiltration studies, GFP expressing animals were obtained from Rat Resource and Research Center (RRRC) Columbia, MO, USA strain SD-Tg (UBC-EGFP) 2BalRrrc, common name SD-EGFP. GFP expressing animals used in the study were heterozygotes from breeding SD-EGFP with SD animals obtained from Charles River.

3.2. Surgery and post-operative care

Before surgery, animals were acclimatized to standard laboratory conditions and given free access to rat chow and water. The surgical approach for exposing the sciatic nerve, length and location of the segment excised from the sciatic nerve, the type and location of closing-up sutures, anesthesia and perioperative management were similar to previously described studies [10] (Fig. 1). Post-operatively, animals were observed at least daily and treated with a single injection of baytril (5 mg/Kg) for up to 3 days following surgery, acetaminophen (64 mg/kg/day) for up to 7 days following surgery and buprenorphine (2×/day, 0.01–0.05 mg/Kg) for up to 3 days following surgery. Sterile paper rolls and sunflower seeds were offer *ad libero* to the animals for environmental enrichment. There was no autophagy or death that occurred in any of the animals during all experiments.

Table 1
Group study design.

Time line	Treatment	Animals per group
D3	Autograft	4
	Allograft	5 (4 GFP- and 1 GFP+ transplant)
D7	Autograft	4
	Allograft	5 (4 GFP- and 1 GFP+ transplant)
D14	Autograft	4
	Allograft	5 (4 GFP- and 1 GFP+ transplant)
D28	Autograft	4
	Allograft	5 (4 GFP- and 1 GFP+ transplant)
W14	Autograph	4
	Allograft	4

3.3. Electromyography (EMG) to measure CMAPs

CMAPs were measured as described for Clements et al. 2016 study [10]. Briefly, rats were anesthetized with isoflurane 2.5% and Viking-Quest (Natus Neurology) was used to measure CMAPs of left peroneal and tibial muscles by surface stimulation near the heel, targets of the peroneal and sciatic branches of the sciatic nerve. The rats were positioned in decubitus frontal on the working platform in order to measure compound muscle action potentials (CMAP) by EMG. The electrode was placed in the posterior muscles group of the distal region after surgery and the sciatic nerve branches were stimulated at least 6 times with the surface electrode. The reported findings are the average of the 3 largest CMAPs for each animal at each time point. The electrical stimulation parameters were stimulus frequency 1 Hz, intensity lower than 24 mA.

3.4. Nerve collection and euthanasia

AVWA Guidelines for the Euthanasia of Animals and NIH Guide for the Care and Use of Laboratory Animals were followed. Nerves were fixed in situ by exposing the nerves in isoflurane-anesthetized animals and bathing the nerve in Trumps fixative for 30 min. Nerves were then excised from the animals and placed in Trumps fixative.

3.5. Muscle wet weight analysis

For muscle wet weight analysis Wang et al. (2017)'s protocol was followed [11]. Briefly, Tibial anterior and gastrocnemius muscles were dissected and isolated from right and left sides immediately after animals were sacrificed, and weighed using a microbalance (Mettler Toledo, Columbus, OH, EUA). Affected side and unaffected side muscle wet weight values were compared and analyzed for each time point.

3.6. Sectioning and histology (immunohistolochemical analysis)

3.6.1. Tissue processing

Sciatic nerves were harvested, kept in Trump's fixative solution overnight and incubated in 20% sucrose solution for at least 16 h for cryoprotection. Samples were embedded in OCT Cryo mount® (Histolab products AB, Gothenburg, Sweden) and frozen at −20 °C. The nerves were cut in 8–10 μm thin longitudinal sections in a cryotome and collected on superfrost plus glass (Thermo scientific, Braunschweig, Germany) [12].

3.6.2. Immunohistochemistry

Immunohistochemistry in frozen sections was performed for the following antibodies: Anti-Glial Fibrillary Acidic Protein (GFAP), polyclonal (Millipore cat#AB5541, 1:300); Anti-β III Tubulin, polyclonal (Millipore cat# AB9354, 1:50); Anti-rat CD4 PE (cat#12–0040-82, 1:50), Anti-CD3 (Santa Cruz sc-20,047, 1:50); Anti-CD8 (Santa Cruz sc-1177, 1:50); FITC conjugated anti-mouse/human CD45R (B220) antibody (eBioscience cat# 11–0452-81, 1:50); Alexa Fluor 488 conjugated anti-rat CD25 (cat# 202108); Anti-NKp46 (CD335) Antibody, clone WEN23 (Millipore, cat# MABF1970, 1:50); Anti-CD11c Antibody (mouse), PE, clone N418 (Millipore, cat# MABF532, 1:50); Anti-Integrin αM [CD11b] Antibody, clone OX-42, FITC conjugated (Millipore cat# CBL1512F, 1:50).

10 μm longitudinal cryosections were cut in cryostat and mounted on Superfrost Plus glass slides (VWR, Denver, CO, USA). Sections were washed 3× with PBS, followed for 1 h in block solution (5% BSA with 0.1% of triton X) and incubated with primary or conjugated antibody for 1 h at room temperature, washed three time using PBS, and the incubate in secondary antibody (one of the follow antibodies: Alexa flour 555 goat anti-chicken cat# 2437, Goat anti-chicken secondary FICT cat# NB7294, Alexa flour 555 goat anti-mouse cat# A21127, Alexa flour 488 goat anti-mouse cat# A21121; 1:500), lastly DAPI (cat# 62248, Thermo Scientific) was added for 5 min in each section.

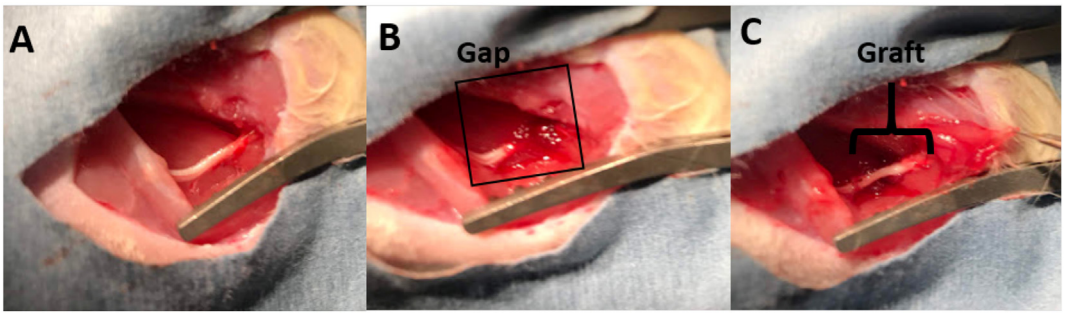

Fig. 1. Sciatic nerve surgery- (**A**) Left sciatic nerve was dissected and (**B**) bisected and 1 cm in length was removed in order to create a gap defect that was (**C**) reconstructed with PN autologous graft, as control groups or with allograft nerve.

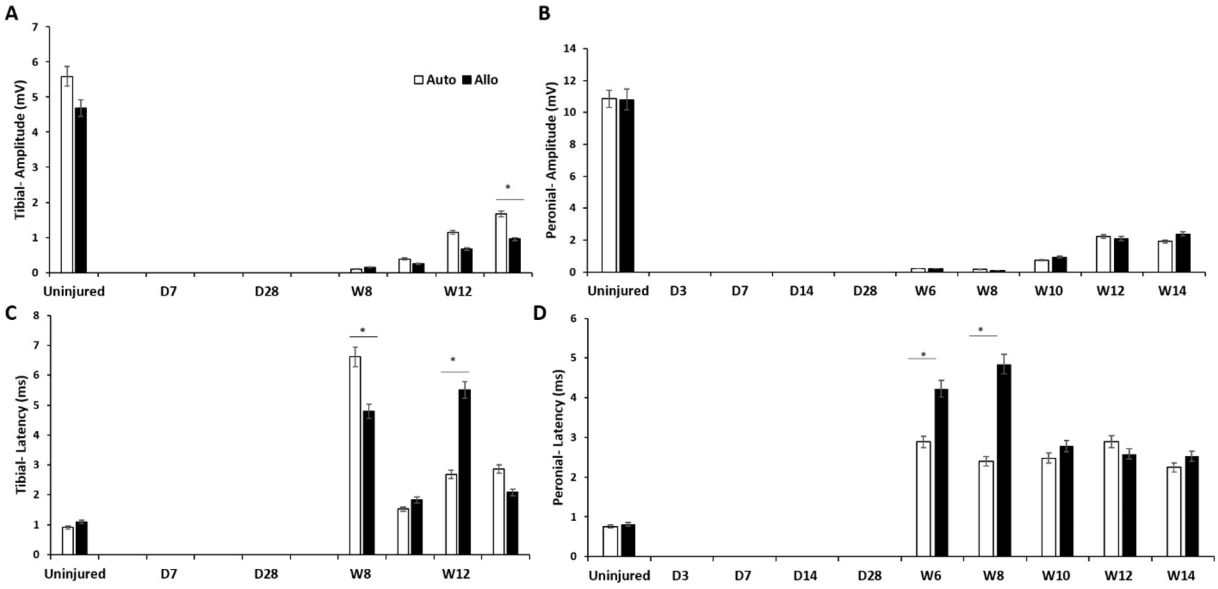

Fig. 2. CMAP results over time on autograft and allograft sciatic nerve graft transplant- Electrophysiological amplitude and latency of nerve conduction were measured for animals the received autologous or allogeneic PN grafts and no immunosuppressive therapy. (A-B) CMAP amplitudes show significant differences for tibial amplitudes but not peroneal amplitudes. (C-D) CMAP latencies indicate slower conduction time for allograft-treated animals at earlier time points. Error bars depict standard error, where $n \geq 4$, $^*p \leq .05$ using analysis of variance (ANOVA) followed by Tukey's test when *P*-values were significant.

3.6.3. Immunofluorescence measurement

First, from each animal at least five frames were taken using Confocal and EVOS FL (life technology, Carlsbad, CA, USA) microscopes in the Jenkins Microscopy Facility at the University of Wyoming at 20× magnification for each antibody from the proximal stump/junction in different regions were taken. In sequence, photomicrographs were analyzed using Confocal and EVOS FL (life technology, Carlsbad, CA, USA) microscopes and image J software. Lastly, the mean grey value of each antibody/marker (integrated density (%)) was obtained by using measurement function of image J software according to published procedures [13–16]. From each photomicrography an average of mean grey value was used for analyzes. This method was used to quantify with accuracy the approximated positive cell number for each antibody/marker in the proximal stump/junction (Supplementary Fig. 1).

3.6.4. Cell infiltration tracking using GFP model

For cell migration analyzes of host/donor, 5 females Sprague–Dawley GFP + were submitted to full transfection sciatic nerve surgery and received 1.0 cm allograft nerve from Lewis rats. Sections were analyzed by microphotography using EVOS FL Color Imaging System (life technology, Carlsbad, CA, USA) microscopes.

3.7. Nerve morphometry

Nerve segments embedding and toluidine blue staining used in this study were according to our previously published protocol [17]. Nerve segment 2 was used for total number of axons, myelinated axon density, percentage of myelinated axons and G-ratio measurement and pathological nerve analyzes.

3.8. Statistical analysis

The statistical analyses were performed using GraphPad Prism 6 (GraphPad Software, Inc. San Diego, CA). Analysis of variance (ANOVA) with $P \leq .05$ was used, followed by Tukey's test when *P*-values were significant.

4. Results

4.1. Electromyography (EMG) to measure compound muscle action potential (CMAP)

To determine the degree of functional regeneration, electrophysiological CMAPs were recorded to measure the strength and speed of the electrical signal conducted by the regenerated nerve to enervated muscle targets. CMAPs first became evident at six weeks (W6), where

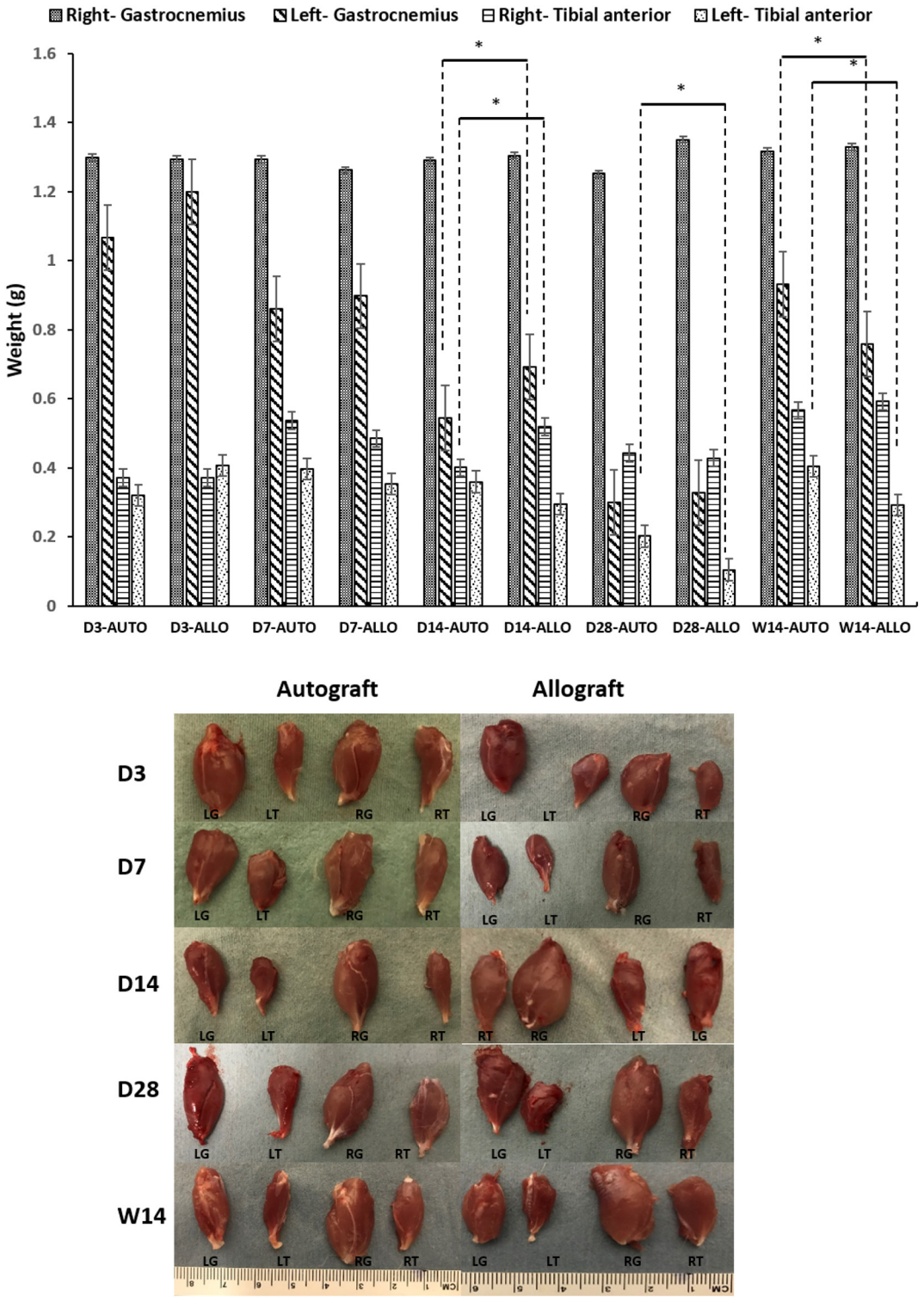

Fig. 3. Muscle wet weight- There was less loss of wet weight of the left tibial posterior muscle on autograft (D28 0.202 g; W14 0.405 g) than allograft group (D28 0.105 g; W14 0.292 g) in special at D28 and W14 as shown in the graft and muscle photographs. Furthermore, autograft group showed heave muscles in the surgical side over time than allograft. Error bars depict standard error, where $n \geq 4$, $^{*}p \leq .05$ using analysis of variance (ANOVA) followed by Tukey's test when *P*-values were significant.

signals were detectable from both autograft and allograft group (Fig. 2). CMAP amplitudes were significantly elevated in autograft groups (Fig. 2A, B), particularly in the tibial nerve (Fig.2A). CMAP latencies show many similar findings between groups, but several time points for both peroneal and tibial showed allografted with longer latencies (Fig. 2C, D). This data indicates an improved regeneration in autografts, but a strong degree of regeneration occurring in allograft recipients, despite that this is a critical size defect and no immunosuppressive therapy was given.

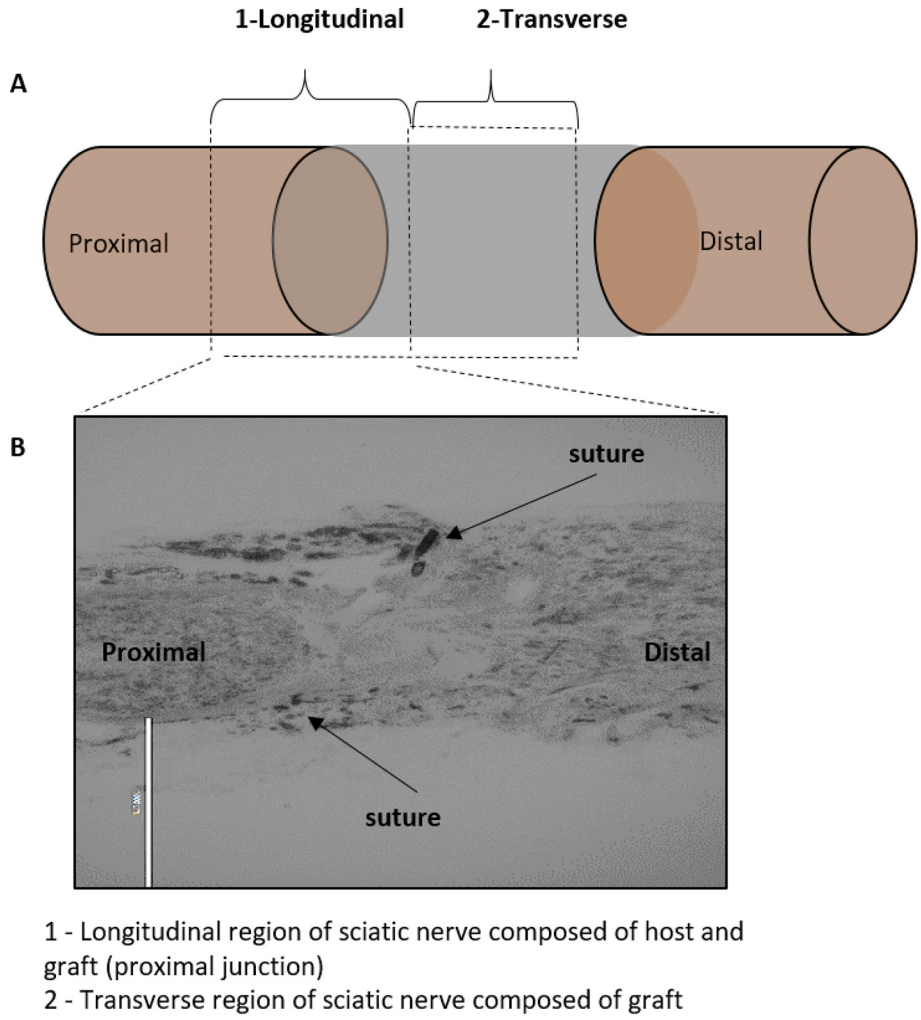

Fig. 4. Sections of nerve analyzed- Nerve was collected from animals and processed for immunohistochemistry and nerve morphometry. (A) Nerve segments encompassing graft (grey) and portions of proximal and distal segments of the host nerve were collected. Segment 1 was analyzed by immunohistochemistry and histology in a longitudinal view while segment 2 was evaluated by cross section and toluidine blue, (B) Image of proximal junction of the host nerve and the graft, using also the sutures to guide the direction and junction region, scale bar = 1000 μm.

Table 2
Markers and cell types assessed in the study.

Antibody	Cell types expressing the markers likely to be found in injured PNs
Glial Fibrillary Acidic Protein (GFAP)	Schwann cells
β III Tubulin	Neurons
CD4	Helper T cells
CD3	T cells
CD8	Cytotoxic T cells
CD45R (B220)	Hematopoietic stem cells, B cell lineage and mature B cell
CD25	Activated T cells, Activated B cells and regulatory T cells.
NKp46	CD3-CD56+ Natural killer cells
CD11c	Monocytes, granulocytes, a subset of B cells, dendritic cells and macrophages
CD11b	Most macrophages and dendritic cells.

4.2. Muscle wet weight analysis

Deinnervated muscles rapidly lose mass and regaining of mass is an indication of functional reinnervation. Muscle mass of the gastrocnemius and tibial anterior muscles are respectively innervated by the peroneal and tibial branches of the sciatic nerve, and muscle mass was measured after euthanasia at the indicated time points. The tibial posterior muscle group lost mass after nerve severing more rapidly than the gastrocnemius (Fig. 3). While some early time points interestingly indicated a more rapid regain of muscle mass in allograft treated groups, this tend had reversed by later time points where autograft muscle mass recovery was significantly elevated over allograft.

4.3. Cell quantification and tracking

4.3.1. Immunofluorescence measurement

To assess cellular infiltration into the graft and regeneration, tissues were collected at D3, D7, D14, D28 and W14 following surgery. For immunohistochemistry, tissue was collected from region 1 of the nerve shown in Fig. 4A and immunostained for the markers indicated in

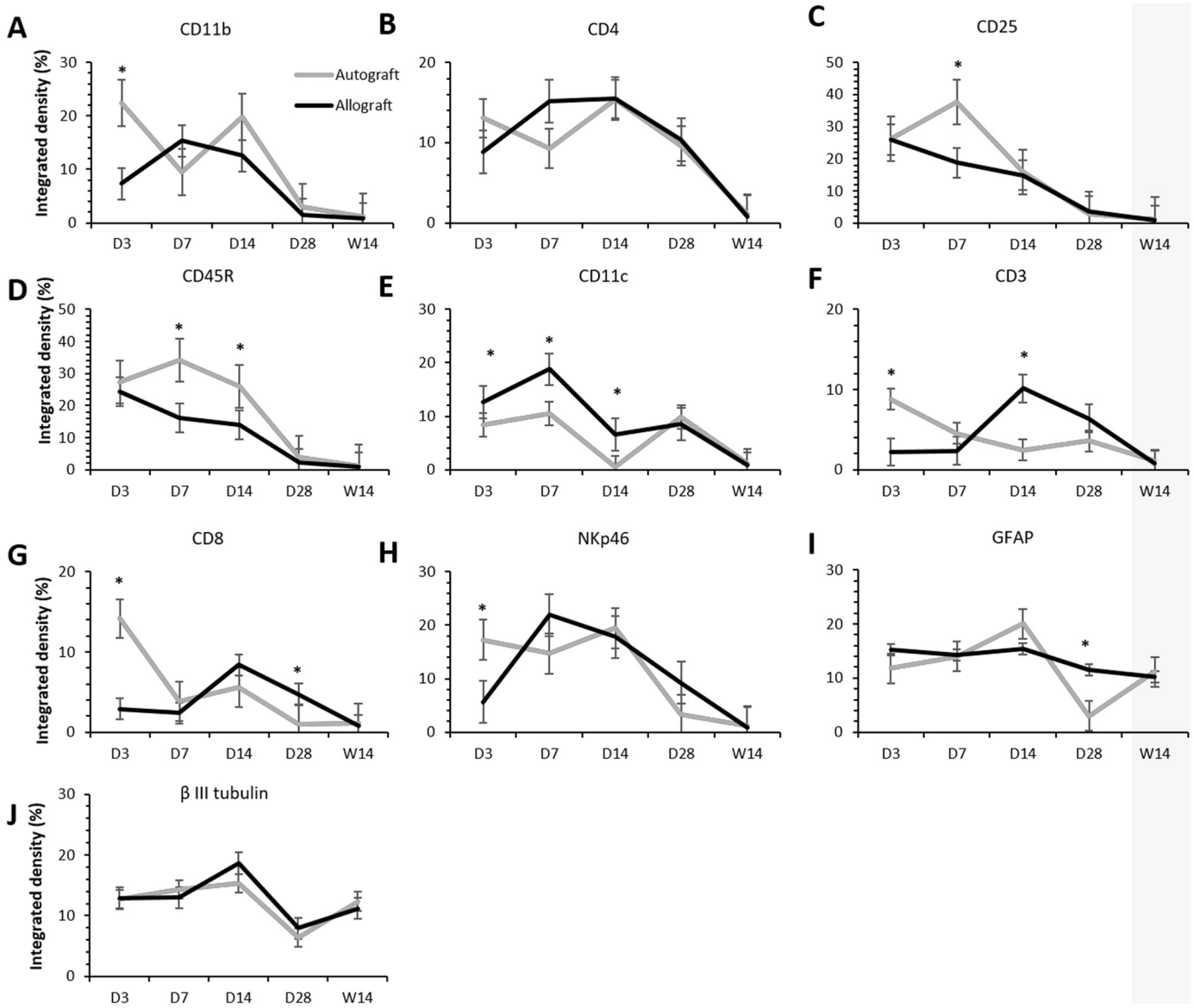

Fig. 5. Quantification of immune and neuronal markers in autograft and allograft- Graphs show integrated density values of (A) CD11b, (B) CD4, (C) CD25, (D) CD45R, (E) CD11c, (F) CD3, (G) CD8, (H) NKp46, (I) GFAP and (J) β III tubulin in autograft and allograft nerve transplant at various time points after implantation. Error bars depict standard error, where $n \geq 4$, $^*p \leq .05$ using analysis of variance (ANOVA) followed by Tukey's test when *P*-values were significant.

Table 2. The host-donor boundary within longitudinal sections collected as described in Fig. 4 could be visualized by the sutures (Fig. 4B) and proximal-distal, host-donor directionality was maintained for all sections to facilitate analysis.

At D3 at the proximal host/donor boundary of autografts, integrated density (%) values, which represent quantity of positive cells, of CD11b (22.049% ± 2.256%), CD3 (8.759% ± 1.347%), CD8 (14.1705% ± 4.446%) and NKp46 (17.27% ± 0.828%), marker was higher than in proximal host/donor boundary of allografts. Values of CD4, CD25, CD45R, GFAP, β III tubulin where similar in both graft types, with no statistic difference, and CD11c (12,693% ± 0,332%) marker was higher in proximal stump of host/allograft (Figs. 5–7).

At D7 in proximal stump of host/autograft CD25 (37.716% ± 6.572%) and CD45R (34.136% ± 0.856%) positive cells were in higher quantity than in proximal stump of host/allograft. Values of CD11b CD4, CD3, CD8, NKp46, GFAP and β III tubulin positive cells were similar in both groups, and CD11c (18.771% ± 9355%) marker was higher in proximal stump of host/allograft (Fig. 5; Supplementary Figs. 2 and 3).

At D14 in proximal stump of host/autograft CD45R (25.856% ± 4.120%) positive cells were in higher quantity than in proximal stump of host/allograft. Values of CD4, CD25, CD8, NKp46, GFAP and β III tubulin were similar in both groups, and values of CD11c (6516% ± 1770%), CD3 (10.118% ± 4.294%) positive cells were higher in proximal stump of host/allograft (Fig. 5; Supplementary Figs. 2 and 3).

At D28 in the proximal stump integrated density (%) values of CD11b, CD4, CD25, CD45R, CD11c, CD3, CD8, NKp46 and β III tubulin were similar in autograft and allograft groups with no statistical difference (Fig. 5; Supplementary Figs. 2 and 3). However, GFAP was higher in the allograft group.

At W14 there was no difference in the integrated density (%) values of all immune cells markers in both groups, but GFAP and β III tubulin values increased in proximal stump of host/allograft and host/autograft groups (Fig. 5; Supplementary Figs. 2 and 3).

4.3.2. Cell infiltration using the GFP model

To assess the migration of donor cells into graft tissue, GFP- grafts

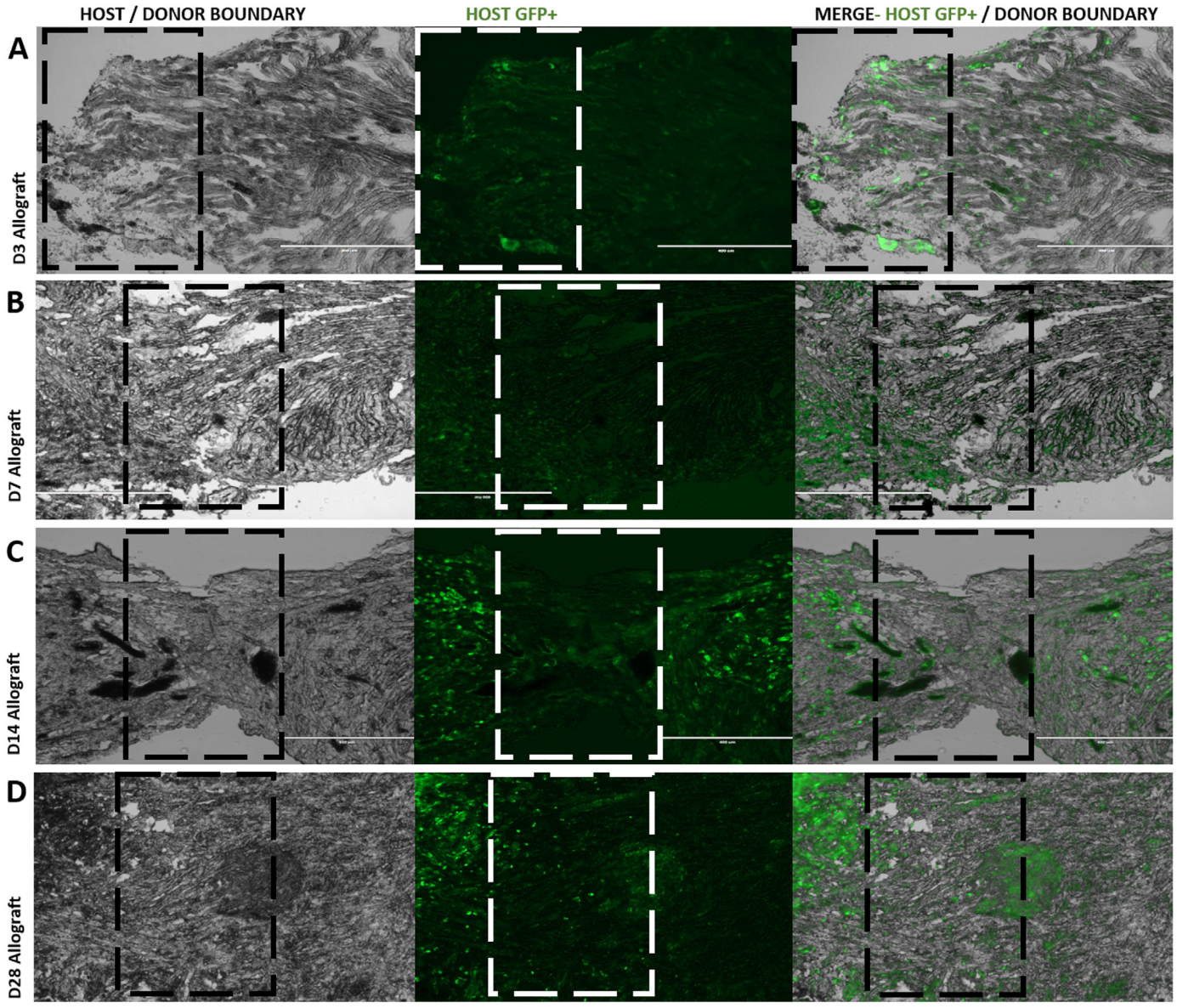

Fig. 6. Cell migration host proximal stump to donor graft- Grafting of GFP- allografts into GFP + hosts shows cellular infiltration. (A) At D3, some migration was observed. An expressive increase was at (B) D7, (C) D14 and (D) D28, dashed squares indicate boundary region, scale bar = 400 μm.

were sutured into GFP + donor animals and the tissue was collected at D3, D7, D14 and D28 post implantation. The presence of GFP + cells in the graft (Figs. 6 and 7) indicated there were cell migration and infiltration from the host to the graft at D3 with an extensive increase at D7, D14 and D28. The host nerve appeared to be a cell pathway guide during this process. Images co-stained for GFAP indicated that Schwann cell migration from host to donor peaked at D14 (Fig. 7). These images also indicate that the vast majority of cells infiltrating the allograft at these time points were not host-derived Schwann cells.

4.4. Nerve morphometry

The middle section of each graft was cross sectioned as indicated in Fig. 4 and stained with toluidine blue to reveal nerve morphometry (Fig. 8A–J). When calculating the total number of axons, there were more axons from D3 to D28 on PN autograft than PN allograft (Fig. 8K). Myelinated axon density showed a significant difference emerged at D7 with more myelinated axons on the autograft until the terminal time point (Fig. 8L). Regarding the percentage of myelinated axons, there were more myelinated axons on allograft from D3 to D14 (Fig. 8M). G-ratio increased over allograft at day 14 (Fig. 8N). This reversed at D28 and both groups displayed similar G-ratios at the W14 terminal time point. This data again indicates improved regeneration in autografts over allografts, but allografts without immunosuppression were still able to stimulate substantial regeneration.

5. Discussion

Nerve regeneration and recovery of function is an orchestrated series of events involving myelin remodeling, axonal regeneration and interactions between PN cells, immune cells, endothelial cells and fibroblasts [5,6,18–20]. In our detailed histological evaluation of the timeline of cell infiltration into PN autografts and allografts, several distinctions between the two emerged as illustrated in supplementary Fig. 4. There were significant elevations in immune cell density in autografts at D3 as compared to allografts, most notably for markers of macrophages and dendritic cells (CD11b), natural killer cells (NKp46) and cytotoxic T cells (CD8 +). The increase in CD3 + in autograft vs allograft was most likely attributed to CD8 + as CD4 + levels did not significantly differ at D3. Previous studies with conduits and coapted

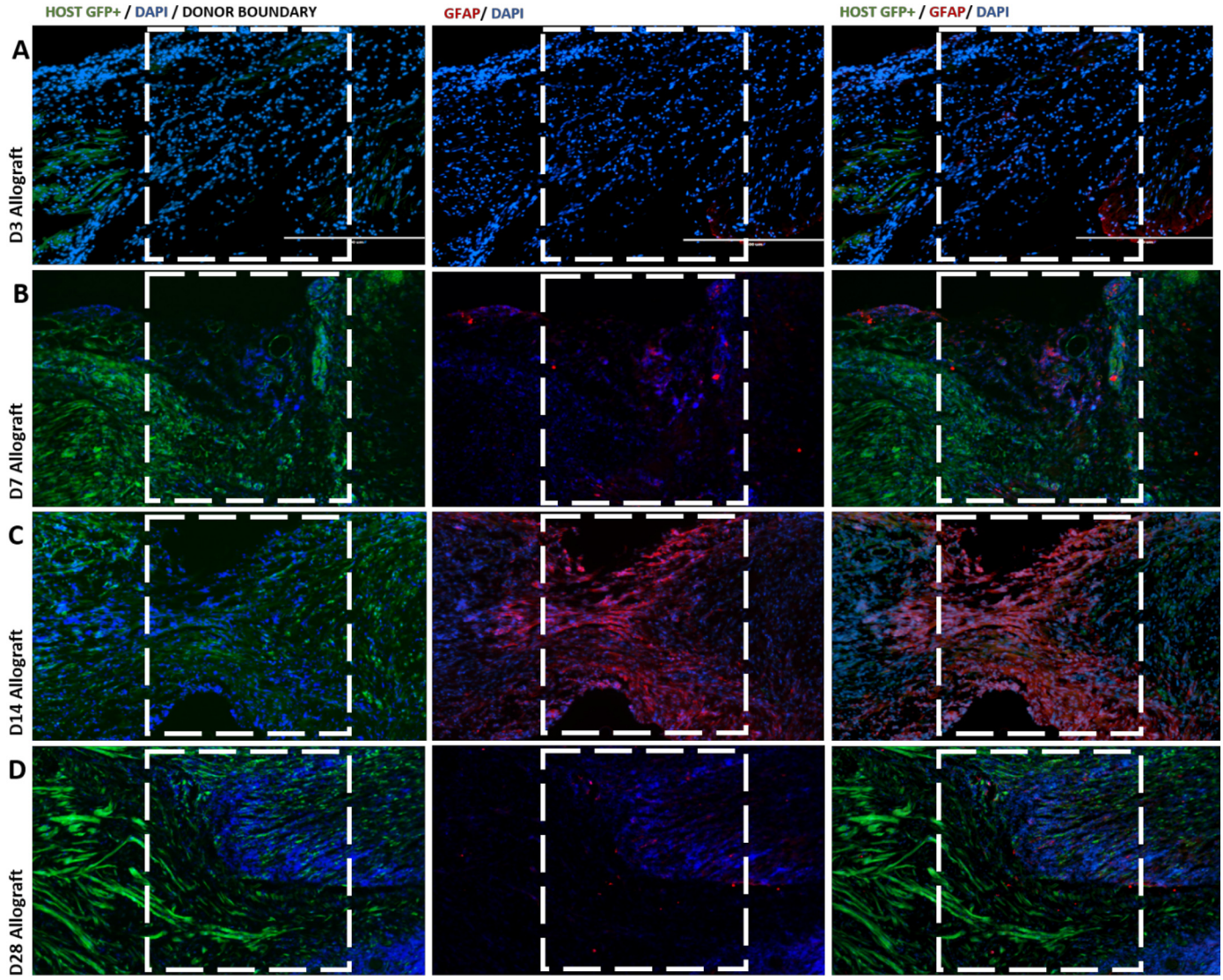

Fig. 7. GFAP positive cells and cell migration host proximal stump to donor graft- Grafting of GFP- allograft into GFP + hosts show GFAP and GFP positive cells in the host and graft proofing GFAP positive cells migrating from the host to the grafting, with a pick at day seven. Some migration was observed at (A) D3, with an expressive increase at (B) D7 and (C) D14 and decrease at (D) D28. Dashed squares indicate proximal host/donor boundary region, scale bar = 400 μm.

bisections affirmed that macrophages accumulate 2–3 days after injury and play an important role in facilitating regeneration [21,22]. From D3 to D28, the cellular response tended to taper downward for all immune cell markers in autografts except for CD25 which spiked at D7. CD25 is a marker of regulatory T cells (Tregs) which may account for this trend as Tregs regulate and inhibit effector T cells and antigen presenting cells [23]. Together, this data suggests that while the early immune response to autografts is more robust than for allografts, the response tapers down over time.

One of the most interesting aspects of the response to allografts was that the presence of effector T cells (CD4 +, CD8 +) was not consistently elevated compared to autograft. Acute graft rejection is primarily mediated by these cell types and as there was no immunosuppression, it was surprising to see that these cell types did not spike in allotransplanted PNs as has been noted for allotransplantation of skin and other tissues [24,25]. This points to a certain degree of immune privilege of PNs and is supported by the functional data; even without immunosuppression, the degree of CMAP (Fig. 2) and muscle mass recovery (Fig. 3) was very close to that of the autografts. Disparities between autografts and allografts generally tended to lessen in magnitude at the later time points, suggesting that continued remodeling and regeneration continue to occur in allografts. Recently published clinical studies also indicate substantial functional regeneration using human cadaveric PN allografts to bridge segmental PN defects without immunosuppressive therapy in humans [26]. While our studies used CMAPs and muscle mass as functional outcomes, this study of 16 patients provided robust sensory and motor outcomes from the patients.

The reasons for this apparent immune privilege are unclear as PN cells and tissue have several immunogenic hallmarks. Within PNs, all nucleated cells would display via MHC I whereas resident macrophages and dendritic cells would be capable of presenting via MHC I and II [27]. In vitro mixed lymphocyte reactions showed mice PN cells to be robustly immunogenic [28]. Schwann cells are one of the most immunogenic of PN cells in these reactions and additionally have the capacity to present antigens via MHC II in certain circumstances [29,30]. Our data shows that T cells accumulate in both autografts and allografts but are only elevated in allografts compared to autografts at D14 for CD3 + and D28 for CD8 + T cells (Fig. 5F, G). In contrast, effector T cells are highly elevated in other transplanted tissues after clonal expansion of allospecific T cells [31,32]. This does not appear to occur to the same extent with PN allografts, suggesting that T cells are

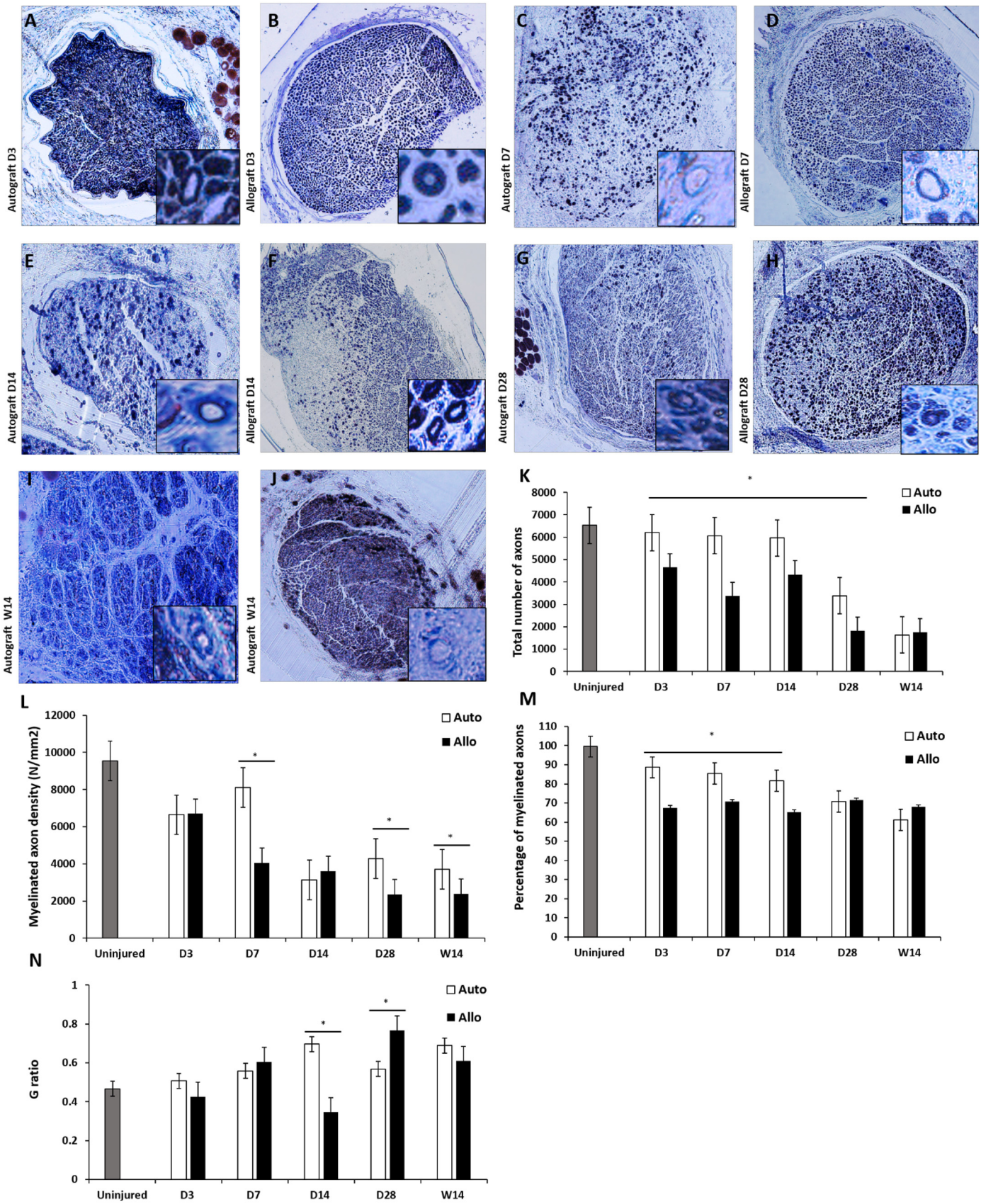

Fig. 8. Morphometry of regenerated nerves within autografts and allografts- (A-J) 10× images of the nerve cables of autograft and allografts at various time points. Inset image is 100×. Quantification of the averages for the groups at each time point shows significant differences between autografts and allografts for (K) total axon count, (L) density of myelinated axons, (M) percentage of axons that were myelinated and (N) G-ratio error bars depict standard error, where $n \geq 4$, $^*p \leq .05$ using analysis of variance (ANOVA) followed by Tukey's test when *P*-values were significant.

accumulating in in both graft types consistent with innate mechanisms of lymphocyte accumulation due to endothelial activation and tissue injury rather than due to MHC-mediated mechanisms [33]. Additional experiments assessing the allospecificity and clonal nature of effector T cells within allografts would help to clarify this issue.

It has been suggested that the immune privilege of allogeneic PNs is due to the epineurium present around PNs, which is may slow immune cell infiltration [34]. We observed that the majority of immune cells infiltrated the graft from the ends, potentially supporting this suggestion that the epineurium is not an accessible route for effector T cell infiltration. However, the extent to which this affects the outcome is unknown as T cells are certainly present in significant amounts within allografts. Another possible explanation would be an over proliferation of Tregs which repress effector T cells [23,35,36], but CD25 did not increase in allografts, suggesting this is not the cause. Our data shows that T cells accumulate within allografts but do not expand to rapidly and robustly eliminate allogeneic cells.

Allogeneic Schwann cells present an interesting case. Previous studies have shown that allogeneic Schwann cells persist for longer than expected after PN allografts [37]. This is paradoxical given the immunogenicity of Schwann cells and our data shows that effector T cell populations are present within allografts. A possible explanation is that donor-derived Schwann cells that successfully remyelinate a host axon may sufficiently reduce their immunogenicity to avoid being targeted by the host immune response. Densitometry of GFAP in our study indicated very little change in GFAP expression in allografts for all time points (Fig. 5I) but did not quantify donor vs host. However, the infiltration studies using GFP hosts indicated a robust amount of host-derived Schwann cells infiltrating the graft at D14 (Fig. 7C). For this degree of infiltration to be occurring and for overall Schwann cell densitometry to remain constant it would suggest donor-derived Schwann cells were being eliminated. Increases in CD3+ and CD8+ cells in allografts at D14 as compared to D3 and D7 would support this (Fig. 5F, G). This potential trade off of donor Schwann cell elimination and host Schwann cell infiltration may be the underlying cause for the delays in functional regeneration that are observed in PN allografts without immunosuppressive therapy in comparison to autografts or allografts treated with immunosuppressive therapy.

The immune response is key for nerve transplant success, but there are other points to consider such as nerve length, vascular microenvironment, stressed cells accumulated in grafting scenarios, which immediately impacts regeneration [38]. In conclusion, the findings exposed in this study suggest that the immune response for PN autografts is rapid in onset and declines thereafter while in PN allografts without immunosuppression the cell-mediated response is slower to accumulate and does not cause additional T cell infiltration as compared to autografts. This lack of a disproportionate T cell -mediated response could be the key for why substantial regeneration and functional recovery occur in PN allotransplants without immunosuppression.

Acknowledgements

The authors would like to thank Dr. Zhaojie Zhang from the Jenkins microscopy facility and the University of Wyoming for support and guidance in fluorescent imaging. We would additionally like to thank Tasneem Hassan Muna and Dr. Adel Ghnenis for editing and proofreading.

Funding sources

This work was funded through the National Institutes of Health (P20GM103432), the Musculoskeletal Transplant Foundation and the University of Wyoming startup funds. The content is solely the responsibility of the authors and does not necessarily represent the official views of the National Institutes of Health, Musculoskeletal Transplant Foundation or the University of Wyoming.

Appendix A. Supplementary data

Supplementary data to this article can be found online at https://doi.org/10.1016/j.trim.2019.01.003.

References

[1] G.A. Grant, R. Goodkin, M. Kliot, Evaluation and surgical management of peripheral nerve problems, Neurosurgery 44 (1999) 825–839.
[2] D. Grinsell, C.P. Keating, Peripheral nerve reconstruction after injury: a review of clinical and experimental therapies, Biomed. Res. Int. 2014 (2014) 698256, https://doi.org/10.1155/2014/698256.
[3] S. Sunderland, A classification of peripheral nerve injuries producing loss of function, Brain 74 (1951) 491–516.
[4] H.J. Seddon, Surgical Disorders of the Peripheral Nerves, Churchill Livingstone, Edinburgh and London, 1972.
[5] S.K. Lee, S.W. Wolfe, Peripheral nerve injury and repair, J. Am. Acad. Orthop. Surg. (8) (2000) 243–452.
[6] D. McDonald, C. Cheng, Y. Chen, et al., Early events of peripheral nerve regeneration, Neuron Glia Biol. 2 (2006) 139–147.
[7] R. Gaudin, C. Knipfer, A. Henningsen, R. Smeets, M. Heiland, T. Hadlock, Approaches to peripheral nerve repair: generations of biomaterial conduits yielding to replacing autologous nerve grafts in craniomaxillofacial surgery, Biomed. Res. Int. 2016 (2016) 3856262, https://doi.org/10.1155/2016/3856262 (Epub 2016 Jul 31).
[8] T.M. Brushart, J. Gerber, P. Kessens, Y.G. Chen, R.M. Royall, Contributions of pathway and neuron to preferential motor reinnervation, J. Neurosci. 21 (1998) 8674–8681 (PMID: 9786974).
[9] M. Siemionow, E. Sonmez, Nerve allograft transplantation: a review, J. Reconstr. Microsurg. 8 (2007) 511–520, https://doi.org/10.1055/s-2007-1022694.
[10] B.A. Clements, J. Bushman, N.S. Murthy, M. Ezra, C.M. Pastore, J. Kohn, Design of barrier coatings on kink-resistant peripheral nerve conduits, J. Tissue. Eng. 7 (2016), https://doi.org/10.1177/2041731416629471. eCollection 2041731416629471. (2016 Jan-Dec).
[11] G. Wang, L. Cao, Y. Wang, Y. Hua, Z. Cai, J. Chen, et al., Human eyelid adipose tissue-derived Schwann cells promote regeneration of a transected sciatic nerve, Sci. Rep. 7 (2017) 43248, , https://doi.org/10.1038/srep43248.
[12] L. Stenberg, L.B. Dahlin, Gender differences in nerve regeneration after sciatic nerve injury and repair in healthy and in type 2 diabetic Goto-Kakizaki rats, BMC Neurosci. 15 (2014) 107.
[13] M. Geiger, G. Blem, A. Ludwig, Evaluation of imagej for relative bone density measurement and clinical application, J. Oral Health Craniofac. Sci. 1 (2016) 12–21, https://doi.org/10.29328/journal.johcs.1001002.
[14] W.S. Rasband, ImageJ, U. S. National Institutes of Health, Bethesda, Maryland, USA, https://imagej.nih.gov/ij (1997–2016).
[15] C.A. Schneider, W.S. Rasband, K.W. Eliceiri, NIH image to imageJ: 25 years of image analysis, Nature Met. 9 (2012) 671–675.
[16] M.D. Abramoff, P.J. Magalhaes, S.J. Ram, Image processing with ImageJ, Biophoton. Int. 11 (2004) 36–42.
[17] A.B. Ghnenis, R.E. Czaikowski, Z.J. Zhang, J.S. Bushman, Toluidine blue staining of resin-embedded sections for evaluation of peripheral nerve morphology, J. Vis. Exp. 137 (2018), https://doi.org/10.3791/58031.
[18] X.P. Dun, D.B. Parkinson, whole mount immunostaining on mouse sciatic nerves to visualize events of peripheral nerve regeneration, In: Monje P., Kim H. (eds) Schwann Cells. Methods in Molecular Biology, vol. 1739. Humana Press, New York, NY.
[19] A.L. Cattin, A.C. Lloyd, The multicellular complexity of peripheral nerve regeneration, Curr. Opin. Neurobiol. 39 (2006) 38–46.
[20] H.A. Kim, T. Mindos, D.B. Parkinson, Plastic fantastic: Schwann cells and repair of the peripheral nervous system, Stem Cells Transl. Med. 2 (2013) 553–557.
[21] A.L. Cattin, J.J. Burden, L. Van Emmenis, F.E. Mackenzie, J.J. Hoving, N. Garcia Calavia, Y. Guo, M. McLaughlin, L.H. Rosenberg, V. Quereda, et al., Macrophage-induced blood vessels guide Schwann cell-mediated regeneration of peripheral nerves, Cell 162 (2015) 1127–1139.
[22] N. Mokarram, K. Dymanus, A. Srinivasan, J.G. Lyon, J. Tipton, J. Chu, A.W. English, R.V. Bellamkonda, Immunoengineering nerve repair, Proc. Natl. Acad. Sci. U. S. A. 26 (2017) E5077–E5084, https://doi.org/10.1073/pnas.1705757114 (Epub 2017 Jun 13).
[23] H. Zhao, X. Liao, Y. Kang, Tregs: where we are and what comes next? Front. Immunol. 8 (2017 Nov 24) 1578, https://doi.org/10.3389/fimmu.2017.01578 (eCollection 2017).
[24] T. Trumble, R. Gunlikson, D. Parvin, A comparison of immune response to nerve and skin allografts, J. Reconstr. Microsurg. 5 (1993) 367–372.
[25] L. Gallon, O. Traitanon, N. Sustento-Reodica, J. Leventhal, M.J. Ansari, R.C. Gehrau, V. Ariyamuthu, S.A. De Serres, A. Alvarado, D. Chhabra, J.M. Mathew, N. Najafian, V. Mas, Cellular and molecular immune profiles in renal transplant recipients after conversion from tacrolimus to sirolimus, Kidney Int. 87 (2015) 828–838, https://doi.org/10.1038/ki.2014.350 (Epub 2014 Oct 29).
[26] T.L. Carlson, R.D. Wallace, P. Konofaos, Cadaveric nerve allograft: single center's experience in a variety of peripheral nerve injuries, Ann. Plast. Surg. 80 (2018) S328–S332, https://doi.org/10.1097/SAP.0000000000001470.

[27] I. Mellman, S.J. Turley, R.M. Steinman, Antigen processing for amateurs and professionals-Review, Trends Cell Biol. 6 (1998) 231–237.
[28] O. Ishida, M. Ochi, Y. Ikuta, M. Akiyama, Peripheral nerve allograft: cellular and humoral immune responses of mice, J. Surg. Res. 49 (1990) 233–238.
[29] G. Meyer zu Hörste, H. Heidenreich, A.K. Mausberg, H.C. Lehmann, A.L. ten Asbroek, J.T. Saavedra, F. Baas, H.P. Hartung, H. Wiendl, B.C. Kieseier, Mouse Schwann cells activate MHC class I and II restricted T-cell responses, but require external peptide processing for MHC class II presentation, Neurobiol. Dis. 37 (2010) 483–790, https://doi.org/10.1016/j.nbd.2009.11.006 (Epub 2009 Nov 13).
[30] G.M. Zu Horste, H. Heidenreich, H.C. Lehmann, S. Ferrone, H. Hartung, H. Wiendl, B.C. Kieseier, Expression of antigen processing and presenting molecules by Schwann cells in inflammatory neuropathies, Glia 58 (2010) 80–92, https://doi.org/10.1002/glia.20903.
[31] M. Yap, S. Brouard, C. Pecqueur, N. Degauque, Targeting CD8 T-cell metabolism in transplantation, Front. Immunol. 6 (2015) 547, https://doi.org/10.3389/fimmu.2015.00547 (eCollection 2015).
[32] H. Robertson, J. Wheeler, J.A. Kirby, A.R. Morley, Renal allograft rejection–in situ demonstration of cytotoxic intratubular cells, Transplantation 10 (1996) 1546–1549.
[33] J. Marino, J. Paster, G. Benichou, Allorecognition by T Lymphocytes and Allograft rejection, Front. Immunol. 7 (2016) 582, https://doi.org/10.3389/fimmu.2016.00582 (eCollection 2016)..
[34] C.J. Klein, Autoimmune-mediated peripheral neuropathies and autoimmune pain, Handb. Clin. Neurol. 133 (2016) 417–446, https://doi.org/10.1016/B978-0-444-63432-0.00023-2.
[35] M.B. Ezzelarab, Regulatory T cells from Allo- to xenotransplantation: Opportunities and challenges, Xenotransplantation 25 (2018) e12415, , https://doi.org/10.1111/xen.12415.
[36] A. Mancusi, S. Piccinelli, A. Velardi, A. Pierini, The effect of TNF-α on regulatory T cell function in graft-versus-host disease, Front. Immunol. 9 (2018) 356, https://doi.org/10.3389/fimmu.2018.00356 (eCollection 2018).
[37] K. Katsube, K. Doi, T. Fukumoto, Y. Fujikura, M. Shigetomi, S. Kawai, Successful nerve regeneration and persistence of donor cells after a limited course of immunosuppression in rat peripheral nerve allografts, Transplantation 66 (1998) 772–777.
[38] G.M. Hoben, E. Xueping, L. Schellhardt, Y. Yan, D. Hunter, A.M. Moore, A.K. Snyder-Warwick, S. Stewart, S.E. Mackinnon, M. Wood, Increasing nerve autograft length increases senescence and reduces regeneration, Plastic. Reconstructive Surgery 1 (2018), https://doi.org/10.1097/PRS.0000000000004759.